The unprecedented 2016-17 Arctic sea ice growth season: the crucial role of atmospheric rivers and longwave fluxes

Bradley M. Hegyi[1*] and Patrick C. Taylor[1]

[1] NASA Langley Research Center, Climate Science Branch, Hampton, Virginia, USA

*Corresponding author: Bradley M. Hegyi (bradley.m.hegyi@nasa.gov)

Abstract

The 2016-17 Arctic sea ice growth season (October-March) exhibited the lowest end-of-season sea ice volume and extent of any year since 1979. An analysis of MERRA2 atmospheric reanalysis data and CERES radiative flux data reveals that a record warm and moist Arctic atmosphere supported the reduced sea ice growth through two pathways. First, numerous regional episodes of increased atmospheric temperature and moisture, transported from lower latitudes, increased the cumulative energy input from downwelling longwave surface fluxes. Second, in those same episodes, the efficiency that the atmosphere cooled radiatively to space was reduced, increasing the amount of energy retained in the Arctic atmosphere and reradiated back toward the surface. Overall, the Arctic radiative cooling efficiency shows a decreasing trend since 2000. The results presented highlight the increasing importance of atmospheric forcing on sea ice variability demonstrating that episodic Arctic atmospheric rivers, regions of elevated poleward water vapor transport, and the subsequent surface energy budget response is a critical mechanism actively contributing to the evolution of Arctic sea ice.

1 Introduction

In recent years, the characteristics of the Arctic sea ice cover have rapidly changed. Most notably, the areal coverage of the September minimum extent has decreased by ~13% decade^{-1} (Cosimo et al. 2008; Meier et al. 2014), leaving the sea ice younger and thinner (Rothrock et al. 1999; Kwok et al. 2009; Meier et al. 2014). One of the important consequences of the reduced Arctic sea ice thickness is that the sea ice has become more sensitive and responsive to dynamic and thermodynamic perturbations (Bitz and Roe 2004), including those from atmospheric variability. Thus, the link between the atmosphere and sea ice variability has become more important. As seen in recent years, regional and Arctic-wide atmospheric variability has influenced the growth of sea ice in fall and winter (Liu & Key 2014; Cullather et al. 2016), contributing to the interannual variability of Arctic sea ice thickness and extent at both the end of the growth season, and in the subsequent melt season (Letterly et al. 2016).

Surface turbulent and radiative fluxes, key components of the surface energy budget, link the Arctic land, ocean, and ice surface to the atmosphere. Climatologically during fall and winter months, surface fluxes transfer energy away from the surface to the atmosphere, facilitating the surface cooling and sea ice formation and growth. In particular, negative net surface longwave (LW) fluxes are associated with fall and winter sea ice growth over established sea ice (Persson 2012) and sea ice formation over open water (along with turbulent fluxes) (Raddatz et al. 2013). Previous studies have linked variability in surface downwelling and net LW surface fluxes with sea ice growth (Persson et al. 2016; Hegyi & Taylor 2017). Variability in the atmospheric state has a large impact on surface LW fluxes and thus the surface radiative cooling rate. The Arctic atmosphere in winter exhibits two dominant radiative states (Stramler et al. 2011; Liu & Schweiger 2017), a radiatively clear state where a large net LW flux is directed away from the surface supporting sea ice growth and a radiatively opaque state where the magnitude of downwelling LW fluxes are large and net LW fluxes are near zero, reducing or halting sea ice growth. Increased downwelling LW fluxes are associated with increased column water vapor content (Raddatz et al. 2013) and increased cloud cover, in particular by increasing the fraction of clouds containing liquid water droplets (Francis and Hunter 2007). A major source of atmospheric water vapor that supports the increased downwelling LW fluxes is transport from lower latitudes, occurring as episodic moisture intrusions (Woods et al. 2013, Park et al. 2015, Woods & Caballero 2016, Mortin et al. 2016). These intrusions are often associated with narrow bands of high-magnitude column water vapor transport, termed Arctic atmospheric rivers for their similarities in structure to atmospheric rivers at lower latitudes (Liu & Barnes 2015).

This report describes the key characteristics of the 2016-17 Arctic sea ice freeze-up season that resulted in the anomalously slow sea ice growth. Described in the subsequent subsections, understanding these key factors provides insight into processes responsible for the recent rapid increases in Arctic surface temperatures and sea ice loss, and the factors that likely contribute to continued Arctic surface warming and sea ice loss. Our results demonstrate that the remote forcing of the Arctic climate system via Arctic atmospheric rivers is an important and active mechanism operating in the Arctic.

2 Results

2.1 2016-17 sea ice growth season: Lowest end-of-season sea ice volume and extent on record

A defining characteristic of the 2016-17 freeze-up season was the slow growth of sea ice in both extent and volume, resulting in the lowest March end-of-season maximum sea ice extent and lowest April end-of-season volume since 1979. The record low end-of-season volume for the year was due to a combination of both a low September minimum sea ice volume at the beginning of the freeze-up season and a slower rate of growth throughout the season (Figure 1a). Both the September minimum sea ice volume and seasonal growth exhibit statistically significant trends since 1979 toward a lower September volume and increased growth rate. However, the trend in growth is less than the trend in September volume (0.06 vs 0.32 km^3*yr^{-1}). Thus, the overall trend is toward a decreased sea ice maximum at the end of the freeze-up season, primarily driven by the decline in the September sea ice volume.

The total Arctic sea ice extent was consistently less than recent averages from October to the end of the freeze-up season in March (Figure 1b). Additionally, there were a total of 15 days from October 1-March 1 in which the total Arctic sea ice extent decreased overall, including 9 days from October 1-February 1, the most days of extent loss for both periods since 1979 (dates for season listed in Supplemental Table 1).

2.2 Warmest atmosphere and highest atmospheric water vapor content since 1979

Associated with the reduced sea ice growth in the 2016-17 season was a warmer and moister atmosphere. As with sea ice volume and growth, surface temperature were the highest since 1980 in the MERRA2 reanalysis data record, in both the 2-meter temperature and surface skin temperature (Figure 1c). Additionally, the total mean atmospheric water vapor content over the Arctic polar cap, as measured by the cap-average precipitable water (PW), was also the greatest since 1980. The monthly average atmospheric surface temperatures and PW were anomalously high in all months, especially in September and October (Figure 1d), coincident with the period of slow sea ice growth relative to climatology in Figure 1b.

2.3 Increased surface longwave fluxes in response to warm and moist atmosphere

Over the period from October-February, the period of the highest growth rate of sea ice extent and volume, the cumulative amount of energy entering the surface over sea ice through LW fluxes from the atmosphere was the highest of any season in the CERES record (since 2000) (Figure 2a). The large amount of energy transferred by downwelling LW fluxes was consistent with the warm and moist Arctic atmosphere during the 2016-17 freeze-up season, since the magnitude of LW fluxes is directly proportional to temperature and water vapor content (e.g. Peixoto and Oort 1992) (Figure 1c). The growth of the cumulative energy input for the 2016-17 freeze-up season relative to other years was especially large in November and December, where the input was 4.3 standard deviations above the 2000-2015 mean on January 1, 2017.

Countering the increased energy input into the surface by downwelling LW fluxes was an increase in upwelling LW fluxes (i.e. output) from the surface to the atmosphere. This increase is consistent with the warmer surface temperatures observed (Figure 1c) and with the negative feedback between surface temperature and upwelling LW surface fluxes observed during non-melt conditions (e.g. Persson 2012). Thus, despite the increased downwelling LW fluxes during 2016-17, the net LW surface flux actually became slightly more negative (i.e. more net flux directed upward), as upwelling LW flux from the surface also increased, in response to increased surface temperatures.

The overall positive seasonal surface cumulative downwelling LW flux anomalies observed in 2016-17 were supported by distinct events of large-magnitude anomalies (Figure 2c). Both anomalous clear-sky fluxes and cloud radiative effects (CRE), which together sum to the total anomalous downwelling flux, contributed to the peak large-magnitude anomalies throughout the season. In October and November, the contribution from CRE was small, thus clear-sky fluxes were the primary contributor to the peaks. In later months, both clear-sky fluxes and CRE equally contributed to the peak positive downwelling LW fluxes. Each period of increased LW fluxes corresponded with a reduced sea ice extent growth (compare Figs. 1b and 2c) and anomalously large PW.

An example of one of these elevated periods of surface LW fluxes, on November 17, 2016 (Arctic surface temperature anomalies exceeded +23 K on this date at some locations), highlights a similar spatial collocation between sea ice extent growth, large PW values, and increased LW fluxes (Figure 3). The downwelling LW flux anomalies in this sector are collocated with a reduction of sea ice volume and extent around that date (Figure 3b and 3c), and also closely collocated with positive PW anomalies. Figure 3a indicates the presence of an Arctic atmospheric river in the sector with the largest PW anomalies. On the previous day, there was a narrow area of intense atmospheric water vapor transport (colored contours in Figure 3a), extending poleward, and collocated with the positive PW anomalies. The sea level pressure pattern supported the atmospheric river with an associated band of winds directed poleward between a surface cyclone near the pole and a high pressure over Siberia. Atmospheric rivers, elevated PW values, and poleward transport from lower latitudes are common features of all 2016-17 reduced-growth periods, especially in the Atlantic sector (see Supplemental Figures).

2.4 Reduced radiative cooling efficiency

Upwelling LW fluxes, along with surface turbulent fluxes, from the surface to the atmosphere are a primary mechanism by which the Arctic surface cools, facilitating sea ice formation. The fraction of upwelling energy from the surface through LW fluxes transmitted to space (i.e. the cooling efficiency defined by Eq. 1, see Data and Methods) is a function of the atmospheric emissivity, which depends on the amount of greenhouse gases in the atmosphere, especially water vapor, and clouds.

The energy input into the atmosphere by upwelling LW surface fluxes (E_{input} in Eq. 1) is shown in Figure 4a. The input of energy from the surface in 2016-17 was the highest value since 2000, 12.4% ($4.17*10^{21}$ J) larger than the minimum value in the period in 2001. The increase in energy transferred to the atmosphere by upwelling LW fluxes is consistent with the observed increase in Arctic surface skin temperatures (Figure 1c).

Concomitant with the increase in energy input from the surface to the atmosphere by upwelling LW fluxes was an increase in energy output by the LW flux at the top of the atmosphere (TOA, E_{output} in Eq. 1). However, the increase in output was less than the increase in energy input. Without considering cloud effects, the LW TOA flux increased only 6.2% ($1.73*10^{21}$ J) relative to the 2001 minimum. Changes in the radiative effects of clouds over the period further reduced the TOA increase between 2001 and 2016, resulting in an overall increase of TOA LW fluxes by 3.6% ($9.68*10^{20}$ J) relative to the 2001 minimum, much less than the increase in energy input to the atmosphere by upwelling surface LW fluxes. The differences between the increases in energy transmitted by upwelling flux at the surface and TOA can be summarized by defining the cooling efficiency of the Arctic atmosphere (Eq. 1, see Data and Methods). Considering all-sky fluxes, the cooling efficiency of the atmosphere in 2016-17 was at a minimum (0.74) compared to the beginning of the period in 2000 (0.81) (Figure 4c). A similar, but smaller decline in clear-sky cooling efficiency also occurred between 2000 and 2016. Spatially on daily time scales, reduced LW cooling efficiency is associated with increased cloud cover and regions of increased atmospheric water vapor. On November 17, 2016, the decrease in LW cooling efficiency was collocated with regions of anomalously high values of PW (Figure 3d).

3 Conclusions

Increased atmospheric water vapor and cloud cover have two important effects on LW fluxes during the Arctic sea ice freeze-up season. First, these mechanisms increase the amount of downwelling LW flux at the surface, contributing an increase in surface temperature. Examples of this during the 2016-17 freeze-up season are found in Figure 2c, where increased downwelling flux due to increased atmospheric water vapor and clouds warmed the surface. Second, these mechanisms reduce the cooling efficiency of the surface and atmosphere through upwelling LW fluxes to space by reducing LW fluxes at TOA. Together on both daily and seasonal time scales, these changes indicate that the excess energy stored in the surface and released during the freeze-up season is increasingly retained in the Arctic climate system and does not escape to space. The 2016-17 sea ice growth season serves as a prime example of the influence of atmospheric LW fluxes and cooling efficiency on sea ice extent and volume growth.

Our results highlight the increasing importance of atmospheric forcing on sea ice variability. Therefore, we contend that accurate predictions of seasonal variability and long-term trends in Arctic sea ice volume and extent require accurate simulations of atmospheric circulation changes, the surface energy budget, and atmosphere-sea ice coupling. In order to improve predictions of sea ice variability and long-term trends we must refine our understanding of the mechanisms that contribute to sea ice growth and melt. Our results demonstrate that Arctic atmospheric rivers and the subsequent response of the surface energy budget is a critical mechanism contributing to the evolution of Arctic sea ice, including extremes in individual sea ice growth seasons such as 2016-17. While this analysis cannot not strictly argue that remote mechanisms are driving rapid Arctic climate change, our results clearly demonstrate that the remote forcing mechanism via the episodic moisture intrusions is an active mechanism contributing to extreme events in the Arctic climate system.

4 Data and Methods

All atmospheric variables, such as atmospheric temperature and precipitable water quantities, are taken from the NASA MERRA2 reanalysis dataset (Bosilovich et al. 2015). All trends and major results presented are qualitatively similar when other reanalysis datasets, such as the ERA-Interim dataset (Dee et al. 2011), are used to recreate the presented results. For surface and top-of-atmosphere (TOA) radiative flux quantities, we use the CERES-SYN dataset, version 3 (Wielicki et al. 1996), containing daily longwave surface and TOA flux quantities over a 1°x1° grid in both clear-sky and all-sky conditions. Sea ice extent data is taken from Nimbus-7 SMMR and DMSP SSM/I-SSMIS Passive Microwave Data (Cavalieri et al. 1996), and sea ice volume data is taken from the Pan-Arctic Ice-Ocean Modeling and Assimilation System (PIOMAS) dataset (Zhang and Rothrock 2003). When calculating the total energy input/output of LW fluxes at the surface, we consider surface LW fluxes only over areas covered with sea ice at the end of sea-ice growth season. Therefore, when calculating the total energy input/output, we only consider grid points that are north of 65°N latitude and climatologically are sea-ice covered (i.e. climatological sea ice concentration greater than 15%) on April 1.

We define the cooling efficiency of the Arctic atmosphere by LW fluxes as the ratio between the input energy into the atmosphere by upwelling LW fluxes from the surface and the output of energy by LW fluxes at the top of the atmosphere.

$$\boldsymbol{\varepsilon} = \frac{E_{output}}{E_{input}} = \frac{\sum_t \sum_{i,j} LW_{up,TOA} * A_{i,j} * \Delta t}{\sum_t \sum_{i,j} LW_{up,SFC} * A_{i,j} * \Delta t} \qquad (1)$$

The energy output (input) is the product of the upwelling longwave flux at TOA (the surface) in the CERES-SYN dataset, $LW_{up,TOA}$ ($LW_{up,SFC}$), the area of the gridbox ($A_{i,j}$), and the sampling period of the data (Δt). The energy output is then summed over all climatologically sea-ice-covered grid points and over the entire October-February period to find the total energy output (input) for the season. Alternatively, the cooling efficiency can be thought of as the effective transmissivity of the atmosphere to upwelling LW fluxes originating from the surface and escaping to space.

Figures

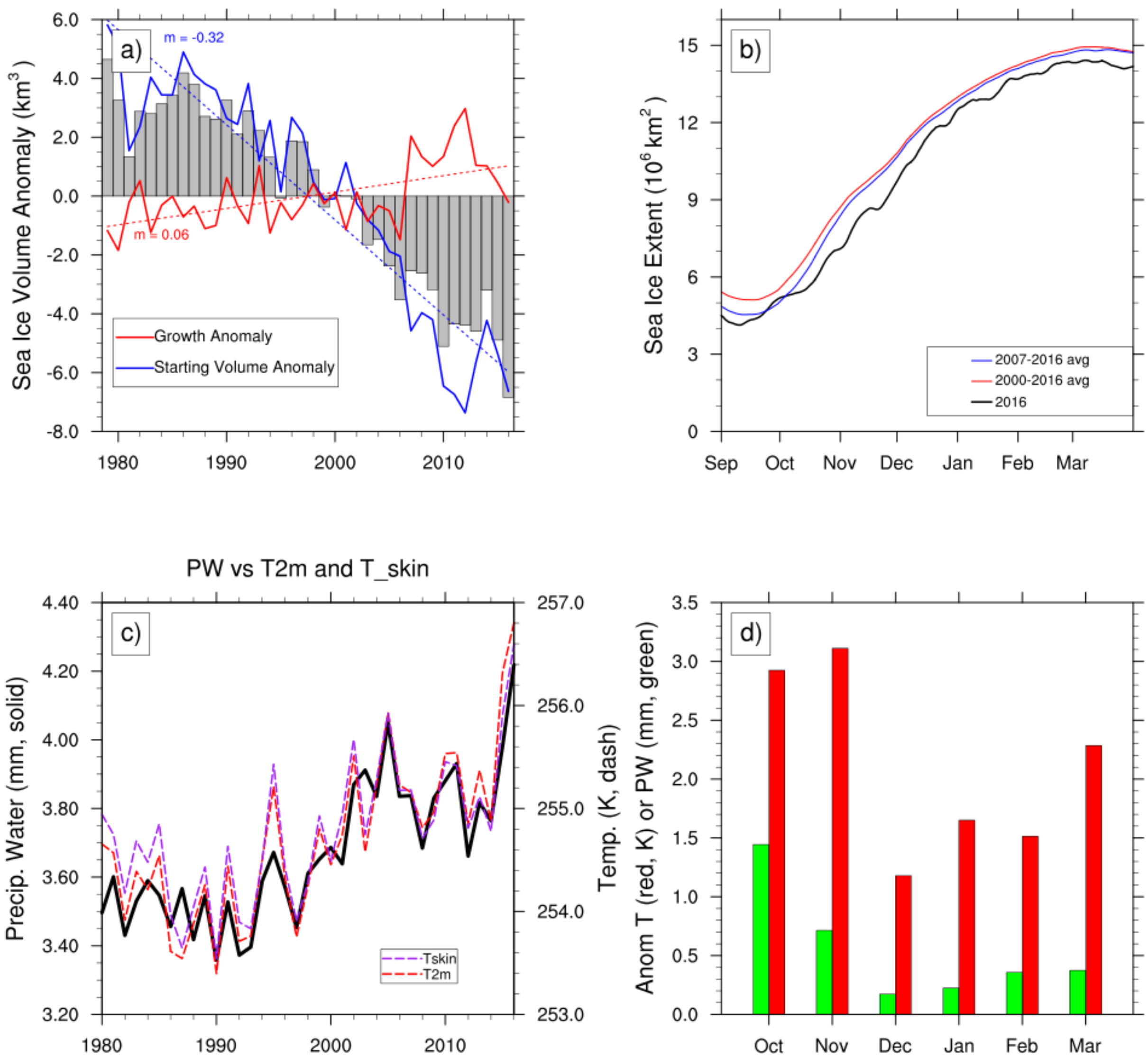

Figure 1. **Comparison of 2016/17 Arctic sea ice growth and atmospheric state to recent years** a) Total sea ice volume anomaly at the end of April across the Arctic north of 65 degrees North (bars). Anomaly is relative to 1979/80-2016/17 climatology in the PIOMAS dataset. The blue line denotes the anomalous volume at sea ice volume minimum in September, and the red line denotes the anomalous growth of sea ice volume from the minimum to the maximum in the September-April period. Linear regression and trend (significant at 99% using modified Student t-test) for datasets represented by lines shown with dotted line. b) Arctic sea ice extent from October-March (units: 10^6 km^2) in 2016 (black line), 2000-2016 average (red line), and 2007-2016 (blue line). c) The Arctic-cap-average precipitable water (solid line, units: mm) and 2-meter temperature (dashed line, units: K) in ONDJF MERRA2 data. d) Anomalous cap-average surface temperature (red bars, units: K) and precipitable water (green bars, units: mm) for

October-February in the 2016-17 season. Anomaly calculated using a 1980/81-2016/17 climatology.

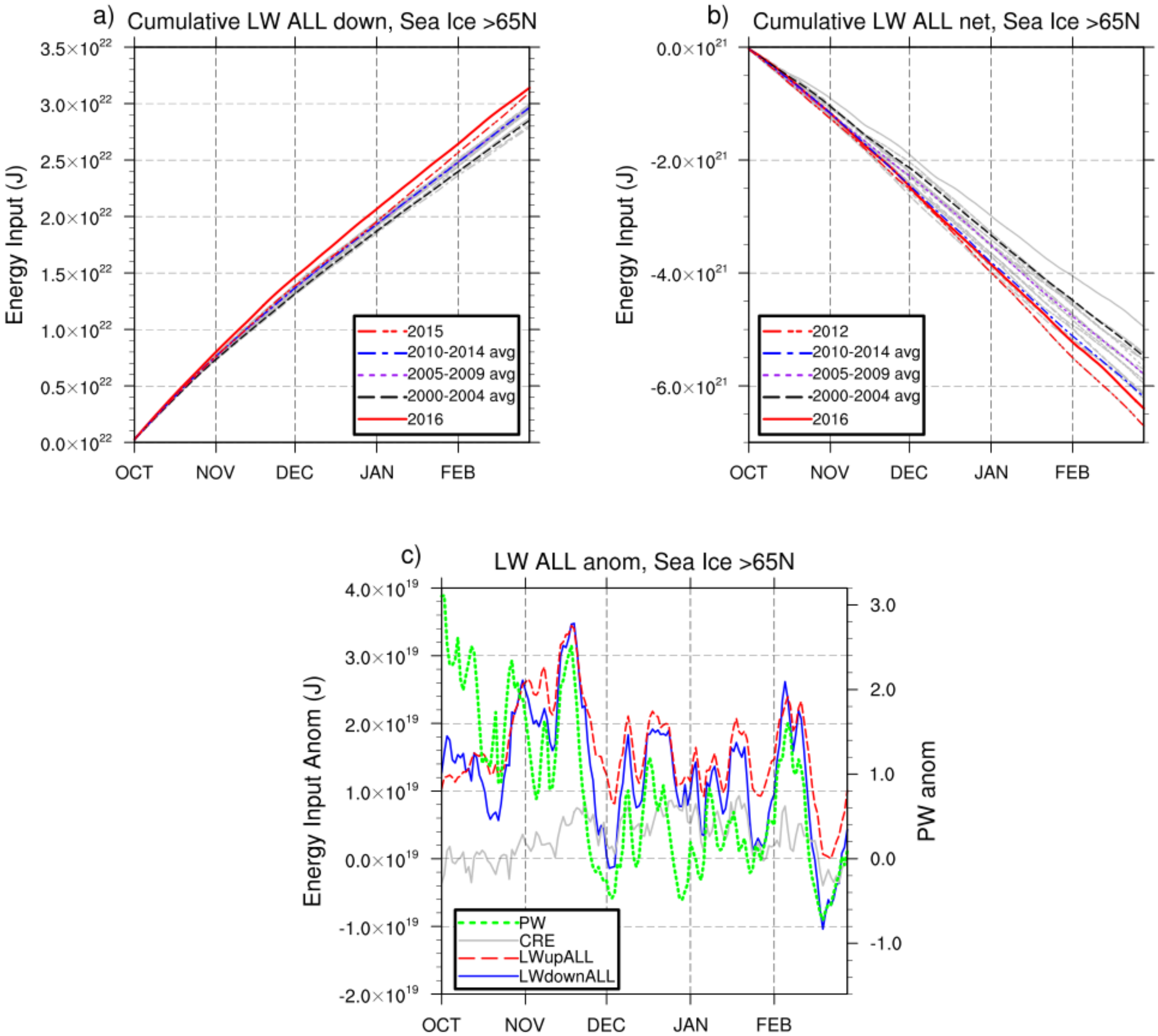

Figure 2. **Evolution of surface longwave fluxes during 2016/17** Cumulative a) downwelling and b) net LW surface fluxes over sea ice areas north of 65°N. Sea ice are is defined as the area with sea ice cover (i.e. sea ice concentration greater than 0.15) on April 1 in a 2000-2016 climatology. b) Same as a), but with the total cumulative energy input/output by net surface LW fluxes. c) Daily surface energy input/output anomalies (units: J) of downwelling surface LW fluxes (blue solid line), upwelling surface LW fluxes (red dashed line), and surface LW cloud radiative effect (CRE, gray solid line) over climatologically sea-ice-covered areas north of 65°N latitude. Also plotted is the mean precipitable water anomaly over the same area (green dotted line).

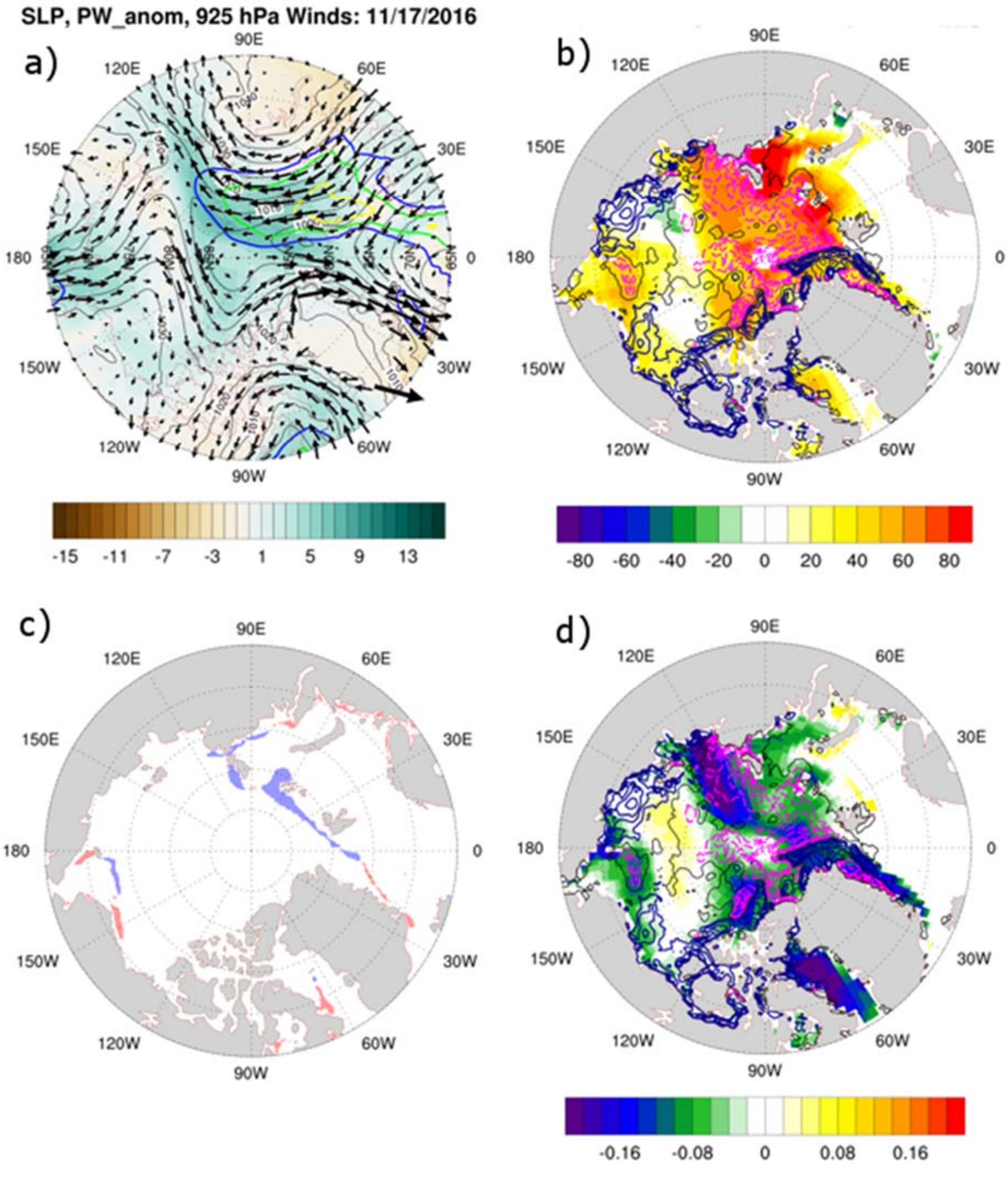

Figure 3. **Spatial distribution of anomalous atmospheric water vapor content, longwave fluxes, and sea ice growth** a) Sea level pressure (contours, units: hPa), anomalous precipitable water (shading, units: mm), and 925 hPa winds on November 17, 2016. Values of total column atmospheric water vapor transport above 100 $kg*m^{-1}*s^{-1}$ on November 16 are also plotted (colored contours with contour interval of 50 $kg*m^{-1}*s^{-1}$) b) All-sky downwelling LW surface flux anomaly (shading, $W*m^{-2}$) on November 17, 2016 and 5-day-mean sea ice volume growth

centered on that date (contours, interval: 0.3 km^3, negative [positive] growth in magenta [blue] contours). c) Changes in sea ice extent on November 15-19, 2016. Red (blue) denotes sea ice extent growth (loss). d) Same as b), but with anomalous cooling efficiency shaded. Only efficiency values over regions ice covered climatologically on April 1 are shown.

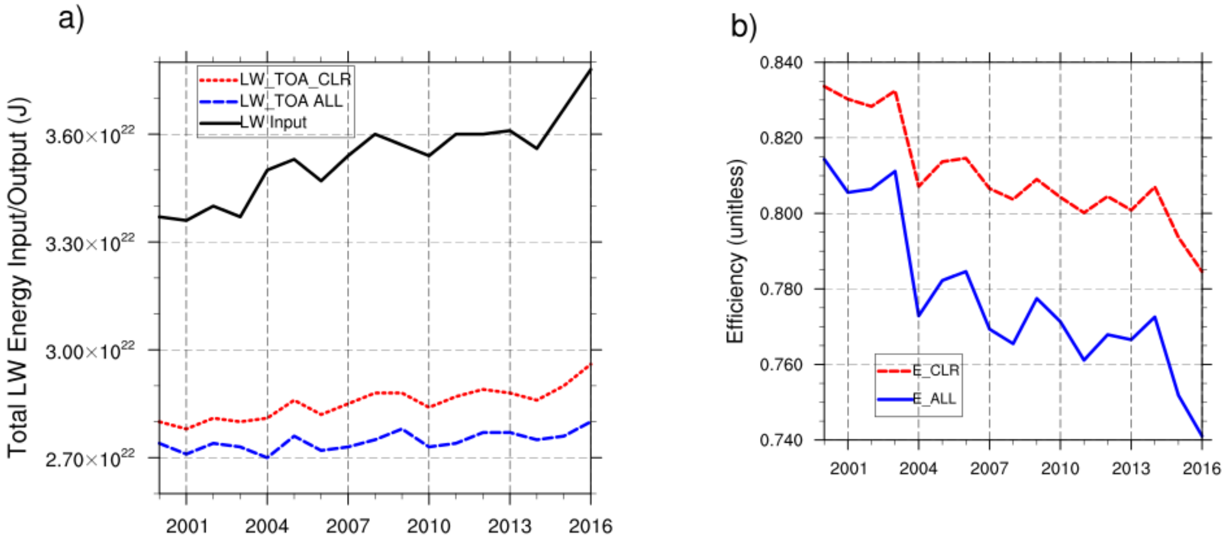

Figure 4. **Longwave cooling efficiency since 2000** a) Total energy input into the atmosphere during October-February (solid black line, units: J) from surface LW fluxes and total energy output (dashed lines, units: J) by TOA fluxes in October-February in clear-sky (red short-dash line) and all-sky (blue long-dashed line) conditions. Energy input and output is calculated over the area north of 65°N that is ice-covered on April 1 in 2000-2016 sea ice cover climatology. b) October-February-mean Arctic cooling efficiency in clear-sky (red line) and all-sky (blue line) conditions for each year in CERES record.

Acknowledgments and Data

CERES-EBAF data were obtained from the NASA Langley Research Center CERES ordering tool at (http://ceres.larc.nasa.gov/). MERRA2 reanalysis data were acquired from the NASA Global Modeling and Assimilation Office (GMAO) and the GES DISC. PIOMAS data was obtained from the website of the Polar Science Center at the University of Washington (http://psc.apl.uw.edu). Bradley M. Hegyi was supported by an appointment to the NASA Postdoctoral Program at the NASA Langley Research Center, administered by Universities

Space Research Association under contract with NASA. This research is also supported by the NASA Interdisciplinary Studies Program grant NNH12ZDA001N-IDS.

References

Bitz, C. M. & Roe, G. H. A mechanism for the high rate of sea ice thinning in the Arctic Ocean. *Journal of Climate* **17**, 3623-3632, doi:10.1175/1520-0442(2004)017<3623:amfthr>2.0.co;2 (2004).

Bosilovich, M.G. et al MERRA-2: Initial evaluation of the climate, Technical Report Series on Global Modeling and Data Assimilation, 43, 139 pg. (2015).

Cavalieri, D., Parkinson, C., Gloersen, P., & Zwally, H.J., Updated yearly. Sea Ice Concentrations from Nimbus-7 SMMR and DMSP SSM/I-SSMIS Passive Microwave Data, Version 1. Boulder, Colorado USA: NASA DAAC at the National Snow and Ice Data Center, doi:10.5067/8GQ8LZQVL0VL. 10 October 2016. (1996).

Comiso, J. C. & Nishio, F. Trends in the sea ice cover using enhanced and compatible AMSR-E, SSM/I, and SMMR data. *Journal of Geophysical Research-Oceans* **113**, doi:10.1029/2007jc004257 (2008).

Cullather, R. I. *et al.* Analysis of the warmest Arctic winter, 2015-2016. *Geophysical Research Letters* **43**, 10808-10816, doi:10.1002/2016gl071228 (2016).

Dee, D. P. *et al.* The ERA-Interim reanalysis: configuration and performance of the data assimilation system. *Quarterly Journal of the Royal Meteorological Society* **137**, 553-597, doi:10.1002/qj.828 (2011).

Francis, J.A. & Hunter, E. Changes in the fabric of the Arctic's greenhouse blanket. *Environmental Research Letters* **2**, 045011, doi:10.1088/1748-9326/2/045011 (2007).

Hegyi, B. M. & Taylor, P. C. The regional influence of the Arctic Oscillation and Arctic Dipole on the wintertime Arctic surface radiation budget and sea ice growth. *Geophysical Research Letters* **44**, 4341-4350, doi:10.1002/2017gl073281 (2017).

Kwok, R. *et al.* Thinning and volume loss of the Arctic Ocean sea ice cover: 2003-2008. *Journal of Geophysical Research-Oceans* **114**, doi:10.1029/2009jc005312 (2009).

Letterly, A., Key, J. & Liu, Y. H. The influence of winter cloud on summer sea ice in the Arctic, 1983-2013. *Journal of Geophysical Research-Atmospheres* **121**, 2178-2187, doi:10.1002/2015jd024316 (2016).

Liu, C. & Barnes, E.A. Extreme moisture transport into the Arctic linked to Rossby wave breaking. *Journal of Geophysical Research-Atmospheres* **120**, 3774-3788 doi:10.1002/2014JD022796 (2015).

Liu, Y. H. & Key, J. R. Less winter cloud aids summer 2013 Arctic sea ice return from 2012 minimum. *Environmental Research Letters* **9**, doi:10.1088/1748-9326/9/4/044002 (2014).

Liu, Z. & Schweiger, A. Synoptic Conditions, Clouds, and Sea Ice Melt Onset in the Beaufort and Chukchi Seasonal Ice Zone. *Journal of Climate* **30**, 6999-7016, doi:10.1175/jcli-d-16-0887.1 (2017).

Meier, W. N. *et al.* Arctic sea ice in transformation: A review of recent observed changes and impacts on biology and human activity. *Reviews of Geophysics* **52**, 185-217, doi:10.1002/2013rg000431 (2014).

Mortin, J. *et al.* Melt onset over Arctic sea ice controlled by atmospheric moisture transport. *Geophysical Research Letters* **43**, 6636-6642, doi:10.1002/2016gl069330 (2016).

Park, H.-S., Lee, S., Son, S.-W., Feldstein, S.B., & Kosaka, Y. The impact of poleward moisture and sensible heat flux on Arctic winter sea ice variability. *Journal of Climate* **28**, 5030-5040, doi:10.1175/JCLI-D-15-0074.1 (2015).

Persson, P. O. G. Onset and end of the summer melt season over sea ice: thermal structure and surface energy perspective from SHEBA. *Climate Dynamics* **39**, 1349-1371, doi:10.1007/s00382-011-1196-9 (2012).

Persson, P. O. G., Shupe, M. D., Perovich, D. & Solomon, A. Linking atmospheric synoptic transport, cloud phase, surface energy fluxes, and sea-ice growth: observations of midwinter SHEBA conditions. *Climate Dynamics* **49**, 1341-1364, doi:10.1007/s00382-016-3383-1 (2017).

Peixoto, J.P. & Oort, A.H., *Physics of Climate Ch. 6* (Springer-Verlag, New York, 1992).

Raddatz, R. L. *et al.* All-Sky Downwelling Longwave Radiation and Atmospheric-Column Water Vapour and Temperature over the Western Maritime Arctic. *Atmosphere-Ocean* **51**, 145-152, doi:10.1080/07055900.2012.760441 (2013).

Rothrock, D. A., Yu, Y. & Maykut, G. A. Thinning of the Arctic sea-ice cover. *Geophysical Research Letters* **26**, 3469-3472, doi:10.1029/1999gl010863 (1999).

Stramler, K., Del Genio, A. D. & Rossow, W. B. Synoptically Driven Arctic Winter States. *Journal of Climate* **24**, 1747-1762, doi:10.1175/2010jcli3817.1 (2011).

Wielicki, B. A. *et al.* Clouds and the earth's radiant energy system (CERES): An earth observing system experiment. *Bulletin of the American Meteorological Society* **77**, 853-868,

Woods, C. & Caballero, R. The Role of Moist Intrusions in Winter Arctic Warming and Sea Ice Decline. *Journal of Climate* **29**, 4473-4485, doi:10.1175/jcli-d-15-0773.1 (2016).

Woods, C., Caballero, R. & Svensson, G. Large-scale circulation associated with moisture intrusions into the Arctic during winter. *Geophysical Research Letters* **40**, 4717-4721, doi:10.1002/grl.50912 (2013).

Zhang, J. L. & Rothrock D. A, Modeling global sea ice with a thickness and enthalpy distribution model in generalized curvilinear coordinates, *Monthly Weather Review*., **131,** 845–861, doi:10.1175/1520-0493(2003)131<0845:MGSIWA>2.0.CO;2 (2003).